DOI 10.2478/ama-2020-0022

FUNCTIONAL BEHAVIOR OF PSEUDOELASTIC NITI ALLOY UNDER VARIABLE AMPLITUDE LOADING

Volodymyr IASNII,[*] Petro YASNIY,[*] Yuri LAPUSTA,[**] Oleg YASNIY,[*] Oleksandr DYVDYK

[*]Department of Structural Mechanics, Ternopil Ivan Puluj National Technical University,
Ruska str. 56, 46001 Ternopil, Ukraine
[**]Université Clermont Auvergne, SIGMA Clermont (ex-IFMA, French Institute of Advanced Mechanics), Institut Pascal,
BP 10448, F-63000 Clermont-Ferrand, France, CNRS, UMR 6602, IP, F-63178 Aubière, France

v_iasnii@tntu.edu.ua, petroyasniy@gmail.com, lapusta@sigma-clermont.fr, oleh.yasniy@gmail.com, sashadyvdyk@gmail.com

Received 24 March 2020, revised 10 November 2020, accepted 13 November 2020

Abstract: Cyclic loading of superelastic NiTi shape memory alloy (SMA) causes forward and reverse austenite–martensite transformations, and also increases the volume of stabilized martensite. This appears in the change of stress-strain curve form, the decrease of dissipation energy, and increase of residual strain, that is, named transformation ratcheting. In real structures, the SMA components in most cases are under the action of variable amplitude loading. Therefore, it is obvious that the loading history will influence the functional fatigue. In the present work, the effect of stress ratio on the functional properties of superelastic NiTi shape memory alloy under variable amplitude loading sequence with two blocks was investigated. The studies were carried out under the uniaxial tension of cylindrical specimens under load-full unload and load-part unload. The change of residual strain, strain range, dissipation, and cumulative dissipation energy density of NiTi alloy related to load sequences are discussed. Under both stress ratios, the residual strain in NiTi alloy is increased depending on the number of loading cycles on the high loading block that is similar to the tests at constant stress or strain amplitude. An unusual effect of NiTi alloy residual strain reduction with the number cycles is found at a lower block loading. There was revealed the effect of residual strain reduction of NiTi alloy on the number of loading cycles on the lower amplitude block. The amount of decrement of the residual strain during a low loading block is approximately equal to the reversible part of the residual strain due to the stabilized martensite. The decrease of the residual strain during the low loading block is approximately equal to the reversible part of residual strain due to the stabilized martensite. A good correlation of the effective Young's modulus for both load blocks with residual strain, which is a measure of the volume of irreversible martensite, is observed.

Keywords: Pseudoelastic NiTi alloy, functional fatigue, variable amplitude loading, strain range, residual strain, dissipation energy

1. INTRODUCTION

Shape memory alloys (SMA) are functional materials, which are characterized by shape memory effect and pseudoelasticity. Due to these properties, they are widely used in bioengineering (Nematollahi et al., 2019), aeronautics (Pecora and Dimino, 2015), robotics (Zeng et al., 2020), and civil and mechanical engineering (Zeng et al., 2020).

Recovery and residual strains are important parameters, which represent a quantitative measure of the cyclic evolution of the SMA pseudoelastic properties during loading. Recovered strain is pseudoelastic recovery from mechanical unloading and residual strain is unrecovered strain upon unloading. The accumulation of inelastic deformation (residual strain) occurring in NiTi shape memory alloy under the cyclic loading is named transformation ratcheting, since it is mainly caused by the solid-solid transformation from austenite to martensite phase and vice versa (Auricchio et al., 2004; Kang, 2013). This evolution associated with deterioration of super-elastic characteristics is referred as "functional fatigue." Recovered and dissipated energy are the parameters that represent the shape of the stress–strain hysteresis loop.

The functional properties of the pseudoelastic SMA deteriorate under cyclic loading (Auricchio et al., 2004; Araya et al., 2008; Kang G., 2013; Vantadori et al., 2018). In particular, there is a significant decrease of recovered strain, recovery energy, dissipated energy, Young's modulus, direct transformation stress, and increased residual strain at strain-controlled and stress-controlled tests (Maletta, 2014; Kang G., 2013).

It is known that the temperature (Araya et al., 2008), type of loading (Mammano and Dragoni, 2012), stress ratio (Iasnii and Yasniy, 2019b; Mahtabi et al., 2015), and heat treatment (Wagner et al., 2008) affect the functional and structural fatigue of SMA.

Most structures and structural elements made of SMA operate under variable amplitude loading at real conditions. However, there exist a few studies regarding the effect of load sequence (Soul and Yawny 2015; Mahtabi at al., 2018) and variable amplitude loading (Soul and Yawny, 2017; Mahtabi et al., 2018) on SMA functional fatigue. In particular, there was studied the effect of various amplitude block loading history under the controlled crosshead displacement on the functional properties of pseudoelastic NiTi alloy (Soul and Yawny, 2017). These blocks were applied with an increasing amplitude sequence, a decreasing amplitude sequence, and interleaved amplitudes. It was shown that the loading type, namely, the block with increasing or decreasing amplitude sequence affects significantly on the residual strain evolution. The linear damage rule cannot be not applied completely to the test full austenite partial martensite (FAPM) cycles, for which the decreasing ordering sequence resulted in lower values

of maximum residual drift (Soul and Yawny, 2017).

Though, it is not clear how the functional properties of superelastic SMA will change after the alternation of blocks with high and low stress amplitude, and different stress ratio. Since degradation or total loss of functional properties may cause failure of a structure, machine or other object, it is important to study the functional behavior of SMA under variable amplitude loading. It is then expected that the global stress–strain response would reflect the previous cycling history of the specimen.

In this paper, the uniaxial functional behavior of superelastic NiTi alloy under two blocks variable amplitude loading was studied experimentally, especially the evolution of the residual strain and energy dissipation of NiTi alloy.

2. MATERIAL AND EXPERIMENTAL SETUP

A commercial pseudoelastic $Ni_{55.8}Ti_{44.2}$ rod (Wuxi Xin Xin glai Steel Trade Co., China) with diameter 8 mm was analyzed. The chemical composition of alloy was given in the paper (Iasnii et al., 2018a). Mechanical properties were determined according to ASTM F2516-14 standard (2014) in ice water at 0°C, which is higher than the austenite finish temperature (A_f = −38.7°C): yield strength, $\sigma_{0,2}$ = 447 MPa, ultimate tensile strength, σ_{UTS} = 869 MPa (V Iasnii et al. 2018a). The phase transformation temperatures were identified as A_s = –60.5°C and A_f = –38.7°C using differential scanning calorimetry by Q1000 TAI during heating and cooling of the specimen (Iasnii and Junga, 2018; V Iasnii et al., 2018b).

The effect of two blocks' variable amplitude loading on functional properties of NiTi alloy under uniaxial tension of the cylindrical specimens with a diameter of 4 mm and a gage length of 12.5 mm at 0°C was investigated. The test technique at constant amplitude loading is described in the paper (Iasnii et al., 2018). Stress-controlled tests were carried out on servo-hydraulic testing machine STM-100 (Yasniy et al., 2005) with automated control and data acquisition system under sinusoidal loading with a frequency of 0.5 Hz. Tests were performed under two blocks variable amplitude loading (Fig. 1a).

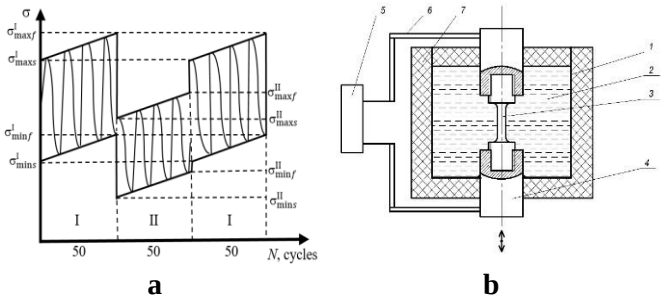

Fig. 1. Loading history (a) and scheme of specimen testing (b):
1 – metal box; 2 – ice and ice water; 3 – specimen; 4 – clamps;
5 – extensometer; 6 – extenders; 7 – insulation wrap

The maximum and minimum loads were increased linearly in each block and jump-like every 50 cycles. This type of loading was chosen due to its similarity with the loading, which undergo the cardiovascular stents in the human body during the change of physical activity (Duerig T. et al., 2003; Pelton, A.R. et al., 2008), the structural elements of bridges due to the change of traffic, and so on. On the one hand, this allows studying the effect of loading history on the functional fatigue of SMA, that is necessary for the physical substantiation and building of SMA fatigue failure models under the variable amplitude loading. On the other hand, the features of functional behavior at variable amplitude loading are important for the design of models of structural fatigue of alloys (Soul H., Yawny A., 2017).

Two series of tests were performed. In the first series, the stress ratio was $R_\sigma = \sigma_{min}/\sigma_{max}$ = 0.09–0.13, and in the second one, R_σ = 0.33–0.51 (here σ_{min} and σ_{max} are the minimum and maximum stresses of loading cycle, respectively). The cyclic loading parameters are given in Table 1: $(\sigma^I_{\min s}, \sigma^I_{\max s}, \sigma^I_{\min f}, \sigma^I_{\max f})$ are the minimum and maximum stresses in the first and last cycle of the first (I) loading block; $(\sigma^{II}_{\min s}, \sigma^{II}_{\max s}, \sigma^{II}_{\min f}, \sigma^{II}_{\max f})$ are the minimum and maximum stresses in the first and last cycle of the second (II) loading block (Fig. 1a). The previously described sequences (Fig. 1a) and stress parameters (Tab. 1) provided the start of the tests from the fully austenitic side (R_σ = 0.09–0.13), and from the fully martensitic side (R_σ = 0.33–0.51). The force, crosshead displacement and longitudinal strain were recorded during the testing. The longitudinal strain was measured by Bi-06-308 extensometer (Bangalore Integrated System Solutions); maximum error did not exceed 0.1%. The crosshead displacement was determined by inductive Bi-02-313 sensor with an error not more than 0.1%. The tests were carried out in the chamber filled with ice and ice water (Iasnii et al., 2018b). Testing scheme is presented in Fig. 1b. This provided the constant temperature of 0°C measured by chromel–alumel thermocouple mounted on the sample with an error not more than 0.5°C.

3. RESULTS AND DISCUSSION

Typical hysteresis loops for different values of the stress range and different number of loading cycles are shown in Fig. 2.

The functional properties of pseudoelastic SMA can be characterized by residual strain ε_{res}. Fig. 3 shows the dependencies of residual strain upon the number of loading cycles at various stress ratio. The residual strain is generally increasing with the increase of loading cycles' number at stress ratio R_σ = 0.09–0.13 and reaches almost 7% before the failure (Fig. 3a). Nevertheless, the increase of residual strain at variable amplitude loading occurs only on the loading block with higher stress amplitude. The larger volume of non-damaged material is included into the transformation during the transition from the lower to the higher loading amplitude. The nature of this process is reflected in the almost constant residual strain rate on block I. This is consistent with the evolution of NiTi alloy residual strain with the number of loading cycles for blocks with an increasing amplitude sequence (Soul and Yawny, 2015). However, with the decrease of the amplitude sequence, the residual strain shows opposite tendency with the number of cycles. The effect of residual strain decrease is observed during the second loading block. This can be caused by the decrease of material volume involved in the transformation and reduction of the residual stresses during the second block. SEM and TEM studies (Hua P. et al., 2020) indicate that cyclic phase transformation results in the formation and glide of transformation-induced dislocations. These dislocations inhibit reverse transformation and result in residual martensite and residual stresses.

It can be assumed that similar to NiTi alloy heating above the austenite transformation finish temperature (Hua P. et al., 2020),

DOI 10.2478/ama-2020-0022

low-amplitude loading triggers reverse transformation of the residual martensite after high amplitude, due to partial reduction of the residual stresses. Obviously, a decrease in residual stress will be accompanied by a decrease in residual strain.

However, this phenomenon requires a more detailed experimental study of functional properties and transformation of the microstructure under variable amplitude loading sequence.

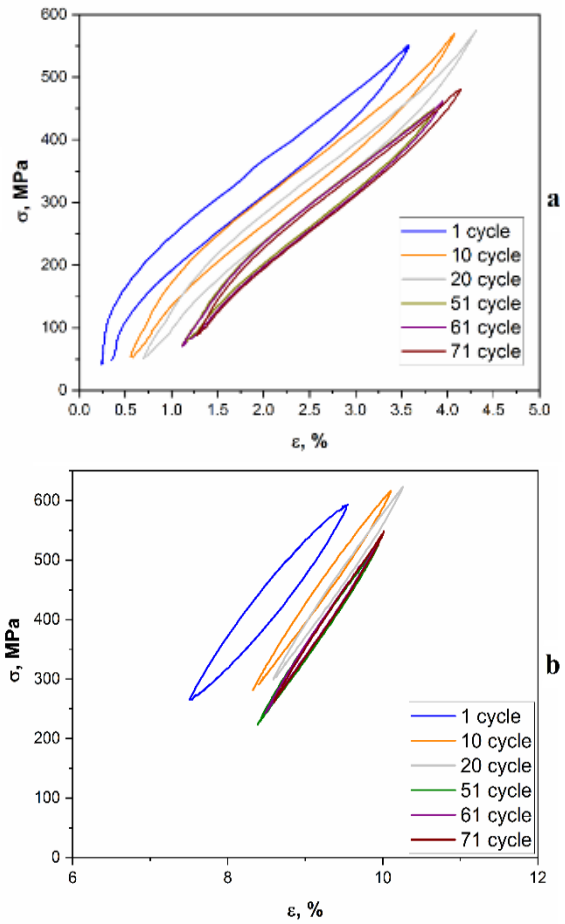

Fig. 2. Typical hysteresis loops for variable loading amplitude at R_σ = 0.09–0.13 (a) and at R_σ = 0.33–0.51 (b)

This regularity is preserved during each block of loading up till specimen failure. Therefore, one can conclude that the stepwise decrease of stress amplitude changes on the opposite the character of residual strain dependency on the number of loading cycles. The above-mentioned regularity was also observed at higher stress ratio (Fig. 3b). The increase of residual strain changes with its decrease on the block of lower amplitude (II) during next 50 cycles of loading. This alternation of the increasing and decreasing blocks is observed in each block of loading up till specimen failure.

Fig. 4 shows the dependence of the residual strain increment on the number of loading cycles in blocks I and II at the end of the corresponding block under variable loading at R_σ = 0.09–0.13. The residual strain increment was calculated as follows:

$$\Delta\varepsilon_{\text{res}} = \varepsilon_{\text{res}}^{f} - \varepsilon_{\text{res}}^{s},$$

where $\varepsilon_{\text{res}}^{s}$ and $\varepsilon_{\text{res}}^{f}$ are residual strains at start and finish of block loading, respectively.

The increment of residual strain in the block with a high amplitude (block I) increases from 0.8% for N = 50 cycles to 1.1% for N = 550 cycles. In block II, the decrement of the residual strain varies from –0.2% to –0.11% and is significantly smaller than those in block I. It was studied that the residual strain consists of two parts: plastic strain (~79% of total) due to dislocations and reversible due to residual martensite (~21%), estimated by the recovered strain after heating (Hua P. et al, 2020). In our case, the decrease of residual strain in block II comprises from 10% to 25% of total residual strain in end cycle of block I. This almost coincides with the reversible part of residual strain. Unlike the stress ratio R_σ = 0.09–0.13, at R_σ = 0.33–0.51, the residual strain at the end and at the start of each block is practically not sensitive to the number of loading cycles (Fig. 3b). This can be explained that in this case, the value of residual strain in the first cycle of loading comprises 8.8%, which exceeds the maximum strain, at which the effect of pseudoelasticity is observed (Iasnii et al., 2018). It is also known that the pseudoelastic deformation of SMA, accompanied with the stress-induced martensitic transformations leads to heat release and, in its turn, it affects the functional properties. The amplitude of the temperature increase becomes more and more significant as the strain level increases (Bubulinca et al., 2013).

It should be noted, that in both cases, the failure of the specimens occurred at the loading block with the higher amplitude.

Tab. 1. The cyclic loading parameters during testing (Fig. 1)

Block	$R_\sigma = \sigma_{min}/\sigma_{max}$	σ_{mins}	σ_{minf}	σ_{maxs}	σ_{maxf}	$\Delta\sigma_s$	$\Delta\sigma_f$	ΔN, cycles
		MPa						
I	0.09–0.10	50	58	530	580	480	522	50
II	0.10–0.13	55	47	430	470	375	423	50
I	0.33–0.43	245	216	572	650	327	434	50
II	0.49–0.51	220	280	450	550	230	270	50

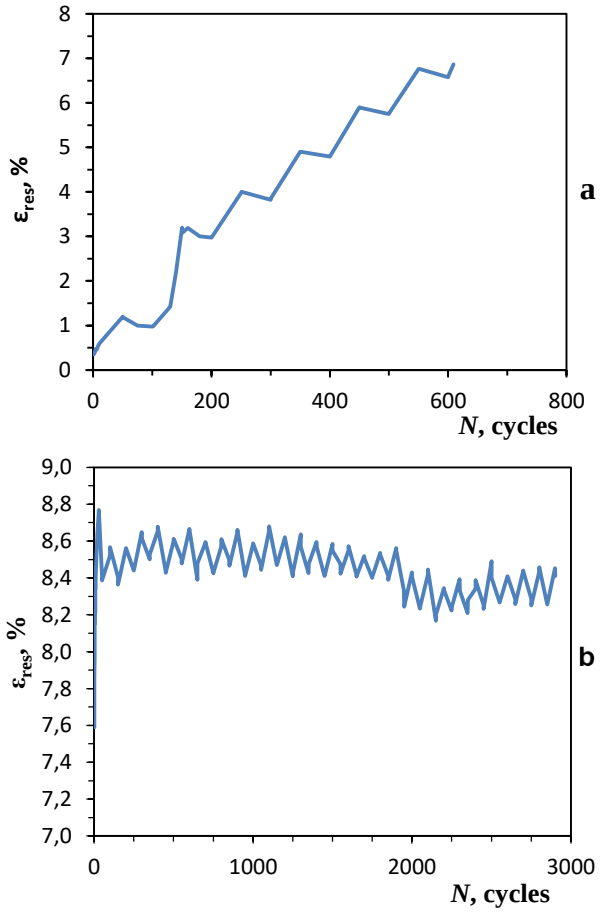

Fig. 3. The dependency of residual strain on the number of loading cycles under variable loading at R_σ = 0.09–0.13 (a) and at R_σ = 0.33–0.51 (b)

The functional properties of pseudoelastic shape memory alloy can be characterized by the strain range per cycle.

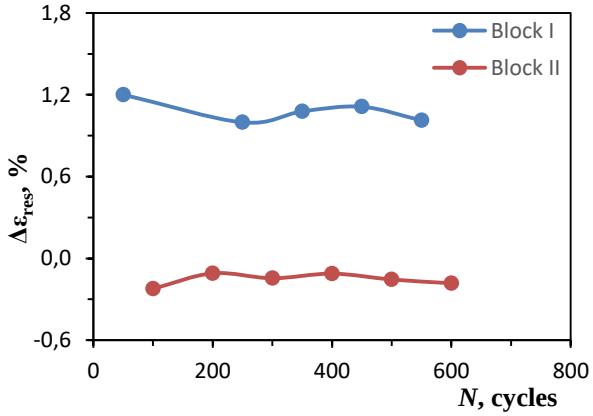

Fig. 4. The dependences of residual strain increment in block I and block II on the number cycles under variable loading at R_σ = 0.09–0.13

Fig. 5 shows the dependencies of minimum and maximum strains (Fig. 5a) and the strain range (Fig. 5b) on the number of loading cycles at R_σ = 0.09–0.13.

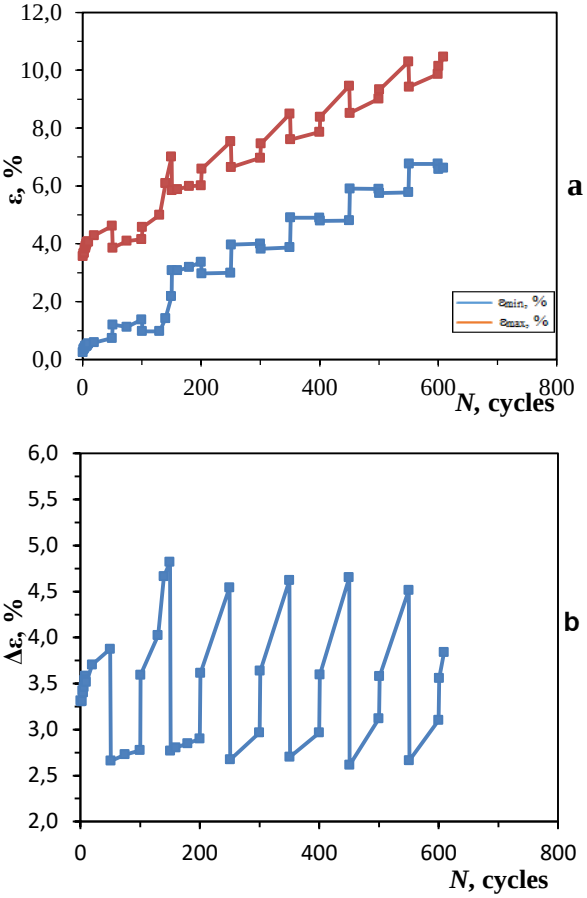

Fig. 5. The dependency of minimum and maximum strain (a) and strain range (b) on the number of cycles under variable amplitude loading at R_σ = 0.09–0.13

Unlike the residual strain, the maximum strain increases with each loading cycle at both loading blocks. Also, the more intensive increase of maximum strain is observed at block I (Fig. 1), that is caused by the interaction effect under the stepwise decrease of specimen loading.

The minimum strain remains invariant to the number of loading cycles within the margins of the first and second block, and the general increase of minimum strain occurs only during the transition from one block to the other. The character of minimum and maximum strain change affects the dependency of strain range on the cyclic loading (Fig. 5b). The mentioned above dependency and the values of the parameters of this dependency within the loading block are almost insensitive to the number of blocks loading up to the specimen failure.

The sawtooth dependency of minimum and maximum strain on the number of loading cycles was observed that was increasing on the first block and decreasing on the second one at two step variable amplitude loading at R_σ = 0.33–0.51, unlike the stress ratio R_σ = 0.09–0.13, (Fig. 5a). This dependency repeats from the loading block to loading block with the constant average strain value. Regardless, some increase of fluctuation of minimum and maximum strain after 2000 loading cycles, this does not affect the dependency of strain range on the number of loading cycles (Fig. 5b). The dependency of strain range on the number of loading cycles and the values of this dependency parameters within the loading block are also almost insensitive to the number of block up to its failure, similarly to the data at values R_σ = 0.09–0.13 (Fig. 4b).

DOI 10.2478/ama-2020-0022

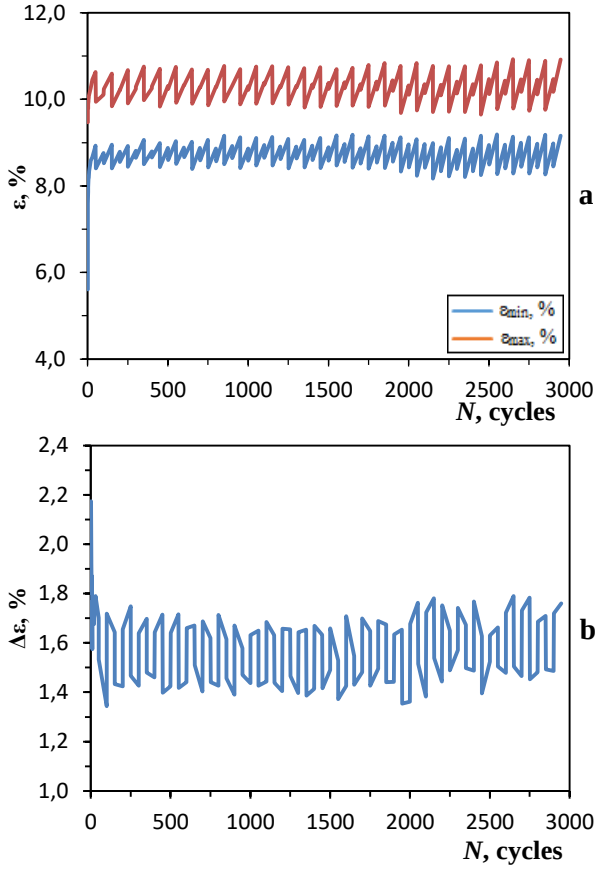

Fig. 5. The dependency of minimum and maximum strain (a) and strain range (b) on the number of cycles under variable amplitude loading at R_σ = 0.33–0.51

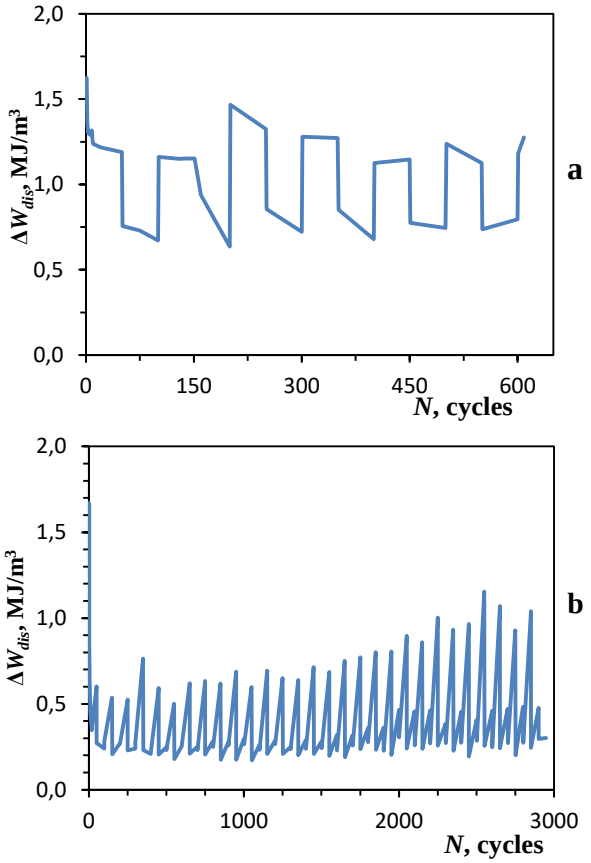

Fig. 6. Dependence of dissipation energy on the number of cycles under variable amplitude loading at R_σ = 0.09–0.13 (a) and R_σ =0.33–0.51 (b)

The dissipated energy per cycle was calculated as difference between the areas under loading and unloading stress – strain curves, using numerical integration. Fig. 6 shows the dependences of dissipation energy on the loading cycle number under variable amplitude loading at stress ratio R_σ = 0.09–0.13 and R_σ = 0.3–0.39. The intensive decrease in the dissipation energy was observed for both values of stress ratio R_σ during twenty loading cycles (block I), followed by stabilizing block. These data are consistent with the results obtained under constant amplitude loading at stress ratio R_σ = 0.1 and R_σ = 0.5 (Iasnii and Yasniy, 2019b).

Subsequently, with increasing the loading cycle number at R_σ = 0.09–0.13, the dissipation energy increases at the start and at the end of second block, and decreases at the beginning and end of the loading unit first block (Fig. 6a).

In contrast, the dissipation energy is proportional to the loading cycles at the beginning and at the end of first block at stress ratio R_σ = 0.33–0.52 (Fig. 6b). The dissipation energy is also proportional to the number of loading cycles within the first block.

Fig. 6 shows the dependences of accumulated dissipation energy on the loading cycle number under variable amplitude loading at stress ratio R_σ = 0.09–0.13 and R_σ = 0.33–0.51.

The total dissipation energy up to *i*-th cycle was determined by formula:

$$W_i = \sum_{i=1}^{N_k} \Delta W_i,$$

where ΔW_i is the dissipated energy for *i*-th loading cycle.

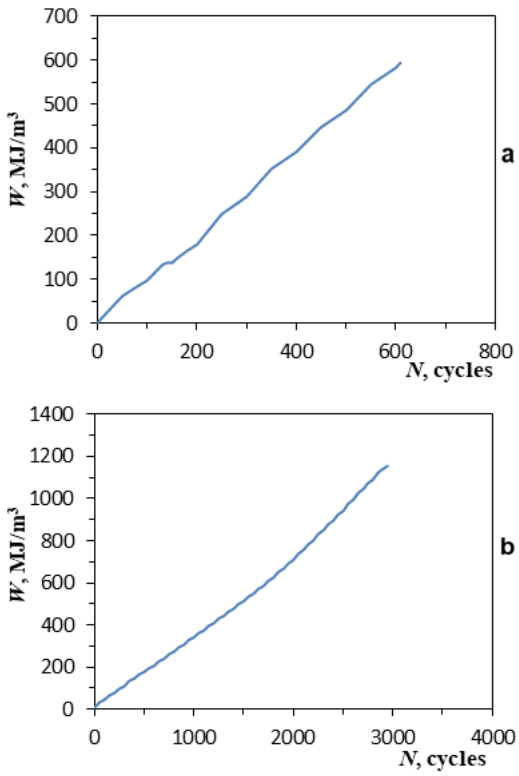

Fig. 7. Dependence of total dissipation energy on the number of cycles under variable amplitude loading at R_σ = 0.09–0.13 (a) and R_σ = 0.33–0.51 (b)

The total dissipation energy increases almost proportionally to the number of loading cycles for both stress ratios. Increasing of stress ratio from R_σ = 0.09–0.13 to R_σ = 0.33–0.51 decreases the total dissipated energy in two times for the same number of loading cycles, but increases the total dissipated energy in more than 3 times up to failure. It should be noted that under the lower value of mean stress, the stress range $\Delta\sigma_f$ exceeds the stress range at R_σ = 0.33–0.51 on the first block of loading spectrum (Fig. 1a) at the R_σ = 0.09–0.13, which determines the intensity of the total dissipation energy increase.

An important parameter that characterizes the functional properties of SMA is Young's modulus of austenite. During cyclic loading the effective Young's modulus decreases due to the increased volume fraction of stabilized martensite.

Fig. 8 shows the dependence of the effective Young's modulus at the last cycle of blocks I and II on the residual strain under variable amplitude loading at stress ratio R_σ = 0.09–0.13.

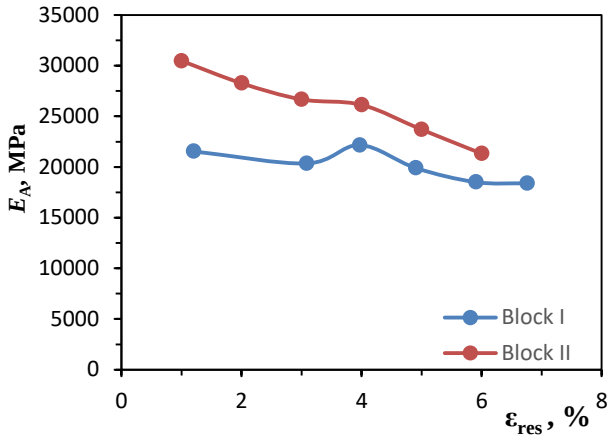

Fig. 8. Dependence of effective Young's modulus austenite in the last cycle of blocks I and II on the residual strain under variable amplitude loading at R_σ = 0.09–0.13

There is observed a good correlation of the effective Young's modulus for both loading blocks with the residual strain, which is a measure of irreversible martensite volume. Increasing the residual stress, the effective Young's modulus decreases in the last loading cycle of blocks I and II. There is a significant difference between the values of the effective elasticity modulus for I and II blocks. At equal residual strain, the effective Young's modulus is smaller at high stress amplitudes. Therefore, the effect of the maximal stress on the effective Young's modulus for a variable amplitude loading at R_σ = 0.09–0.13 is similar to the test at constant strain amplitude (Maletta et al., 2014).

4. CONCLUSIONS

The effect of stress ratio on the functional properties of superelastic NiTi SMA under variable amplitude loading sequence with two blocks at temperature above the austenite finish temperature was studied.

Residual strain significantly increases with the increase of loading cycles number at stress ratio R_σ = 0.09–0.13 and reaches almost 7% before failure. The residual strain is not sensitive to the number of cycles at the end (or start) of loading block under stress ratio R_σ = 0.33–0.51. This can be explained by the fact that in this case, the residual strain in the first cycle is 8.8% that exceeds the maximum strain under which the pseudoelastic effect is still visible.

The dependence of NiTi alloy residual strain on the number of loading cycles increases on the high loading block similarly to the test at constant stress or strain amplitude during both stress ratios.

An unusual effect of functional properties partially recovery – reduce of the NiTi alloy residual strain with the number of loading cycles is found at a lower block loading. It can be assumed that similar to heating of NiTi alloy above the austenitic transformation finish temperature, low-amplitude loading after high amplitude one triggers residual martensite reverse transformation, which partially reduce the residual stresses. The amount of residual strain decrement during a low load block is approximately equal to the reversible part of the residual strain due to the stabilized martensite. This effect can be used to the partial recovery of SMA functional properties.

With the increase of loading cycles' number, the dissipation energy increases at the start and end of block II, and decreases at the start and end of block I at the stress ratio R_σ = 0.09–0.13. In contrast to this, the dissipation energy is proportional to the number of loading cycles at the start and end of block I at stress ratio R_σ = 0.33–0.51. Also, the dissipation energy is proportional to the number of loading cycles within the block I.

Increase of stress ratio decreases the total dissipated energy for the same number of loading cycles, though increases the total dissipated energy up to failure.

REFERENCES

1. **Araya R., Marivil M., Mir C., Moroni O., Sepúlveda A.** (2008), Temperature and grain size effects on the behavior of CuAlBe SMA wires under cyclic loading, *Materials Science and Engineering: A*, 496(1-2), 209–213.
2. **ASTM F2516-14** (2014), Standard Test Method for Tension Testing of Nickel-Titanium Superelastic Materials.
3. **Auricchio F., Marfia S., Sacco E.** (2003) Modelling of SMA materials: training and two way memory effect, *Comput. Struct*. 81, 2301–2317.
4. **Bubulinca C., Balandraud X., Grédiac M., Stanciu S., Abrudeanu M.** (2014), Characterization of the mechanical dissipation in shape-memory alloys during stress-induced phase transformation, *Journal of Materials Science*, 49, 701–709.
5. **Carpinteri A., Di Cocco, Fortese G., Iacoviello F., Natali S., Ronchei C., Scorza D., Vantadori S., Zanichelli A.** (2018), mechanical behaviour and phase transition mechanisms of a shape memory alloy by means of a novel analytical model, *Acta Mechanica et Automatica*, Vol. 12, No. 2, 105–108.
6. **Duerig T., Stoeckel J., Johnson D.** (2002) SMA — smart materials for medical applications, *Proceedings of SPIE 4763*, Bellingham, WA, 7–15.
7. **Hua P., Chu K., Ren F., Sun Q.** (2020), Cyclic phase transformation behavior of nanocrystalline NiTi at microscale, *Acta Materialia*, 185, 507–517.
8. **Iasnii V., Junga R.** (2018), Phase Transformations and Mechanical Properties of the Nitinol Alloy with Shape Memory, *Materials Science*, 54(3), 406–411.
9. **Iasnii V., Yasniy P.** (2019a), Degradation of functional properties of pseudoelastic NiTi alloy under cyclic loading: an experimental study, *Acta mechanica et automatica*, 13(2), 95–100.

10. **Iasnii V., Yasniy P., Lapusta Y., Shnitsar T.** (2018), Experimental study of pseudoelastic NiTi alloy under cyclic loading, *Scientific Journal of TNTU*, 92(4), 7–12.
11. **Iasnii, V., Yasniy P.** (2019b), Influence of stress ratio on functional fatigue of pseudoelastic NiTi alloy, *Procedia Structural Integrity*, 16, 67–72.
12. **Kang G.** (2013), Advances in transformation ratcheting and ratcheting-fatigue interaction of NiTi shape memory alloy, *Acta Mechanica Solida Sinica*, 26(3), 221–236.
13. **Kecik K.** (2015), Application of shape memory alloy in harvesto-absorber system, *Acta mechanica et automatica*, 9(3), 155–160.
14. **Mahtabi M.J., Shamsaei N., Rutherford B.** (2015), Mean strain effects on the fatigue behavior of superelastic Nitinol alloys: An experimental investigation, *Procedia Engineering*, 133, 646–654.
15. **Mahtabi M.J., Stone T.W., Shamsaei N.** (2018), Load sequence effects and variable amplitude fatigue of superelastic NiTi, *International Journal of Mechanical Sciences*, 148, 307–315.
16. **Maletta C., Sgambitterra E., Furgiuele F., Casati R., Tuissi R.** (2014), Fatigue properties of a pseudoelastic NiTi alloy: Strain ratcheting and hysteresis under cyclic tensile loading, *International Journal of Fatigue*, 66, 78–85.
17. **Nematollahi M., Baghbaderani K.S., Amerinatanzi A., Zamanian H., Elahinia M.** (2019), Application of NiTi in Assistive and Rehabilitation Devices: A Review, *Bioengineering*, 6(2), 37.
18. **Pecora R., Dimino I.** (2015), SMA for Aeronautics, *Shape Memory Alloy Engineering*, Chapter 10, 275–304.
19. **Pelton, A.R., Schroeder V., Mitchell M.R., Gong Xiao-Yan, Barney M., Robertson S.W.** (2008), Fatigue and durability of Nitinol stents, *Journal of the Mechanical Behavior of Biomedical Materials*, 1 (2), 153–164.
20. **Scirè Mammano G., Dragoni E.** (2012), Functional fatigue of NiTi shape memory wires for a range of end loadings and constraints, *Frattura ed Integrità Strutturale*, 7(23), 25–33.
21. **Soul H., Yawny A.** (2015), Self-centering and damping capabilities of a tension-compression device equipped with superelastic NiTi wires, *Smart Materials and Structures*, 24(7), 075005.
22. **Soul H., Yawny A.** (2017), Effect of Variable Amplitude Blocks' Ordering on the Functional Fatigue of Superelastic NiTi Wires, *Shap. Mem. Superelasticity*, 3, 431–442.
23. **Wagner M.F., Nayan N., Ramamurty U.** (2008), Healing of fatigue damage in NiTi shape memory alloys, *Journal of Physics D: Applied Physics*, 41(18), 185408.
24. **Yasniy P., Hlado V., Hutsaylyuk V., Vuherer T.** (2005), Microcrack initiation and growth in heat-resistant 15Kh2MFA steel under cyclic deformation, *Fatigue & Fracture of Engineering Materials & Structures*, 28(4), 391–397.
25. **Zeng Z., Oliveira J.P., Ao S. Et al.** (2020), Fabrication and characterization of a novel bionic manipulator using a laser processed NiTi shape memory alloy, *Optics & Laser Technology*, 122.